SECURITY CLASSIFICATION OF THIS PAGE (When Data Entered)

REPORT DOCUMENTATION PAGE

READ INSTRUCTIONS BEFORE COMPLETING FORM

1. REPORT NUMBER: RPI Math. Rep. No. 158
2. GOVT ACCESSION NO.:
3. RECIPIENT'S CATALOG NUMBER:

4. TITLE (and Subtitle): Random-bottom Structural and Topographical Effects on Sound Transmission in a Shallow Channel
5. TYPE OF REPORT & PERIOD COVERED:
6. PERFORMING ORG. REPORT NUMBER:

7. AUTHOR(s): W. L. Siegmann, M. J. Jacobson, and C. E. Ashley
8. CONTRACT OR GRANT NUMBER(s): N00014-86-K-0129

9. PERFORMING ORGANIZATION NAME AND ADDRESS: Rensselaer Polytechnic Institute, Troy, New York 12180-3590
10. PROGRAM ELEMENT, PROJECT, TASK AREA & WORK UNIT NUMBERS: NR 4254007

11. CONTROLLING OFFICE NAME AND ADDRESS: Office of Naval Research, Code 1125UA, Department of the Navy, Arlington, Virginia 22217-5000
12. REPORT DATE: 31 May 1986
13. NUMBER OF PAGES: 34

14. MONITORING AGENCY NAME & ADDRESS (if different from Controlling Office):
15. SECURITY CLASS. (of this report):
15a. DECLASSIFICATION/DOWNGRADING SCHEDULE:

16. DISTRIBUTION STATEMENT (of this Report)

This document has been approved for public release and sale; its distribution is unlimited.

17. DISTRIBUTION STATEMENT (of the abstract entered in Block 20, if different from Report)

18. SUPPLEMENTARY NOTES

19. KEY WORDS (Continue on reverse side if necessary and identify by block number)

Underwater Sound Transmission
Ray Theory
Random Bottom Structure
Random Bottom Topography

20. ABSTRACT (Continue on reverse side if necessary and identify by block number)

Effects of horizontal stochastic bottom structure on acoustic intensity in an isospeed ocean have been studied previously by the authors [J. Acoust. Soc. Am. 76 , 1445-1455 (1984). The bottom density and sound speed were taken to be random and ray theory was used. In this study we add a rough water-bottom interface, consisting of large-scale, two dimensional random facets upon which small-scale roughness may be superimposed. Each facet is assumed to possess

(continued)

DD FORM 1 JAN 73 1473 EDITION OF 1 NOV 65 IS OBSOLETE
S/N 0102-LF-014-6601

UNCLASSIFIED
SECURITY CLASSIFICATION OF THIS PAGE (When Data Entered)

small random depth deviation, slope, and curvature. Initially, we take acoustic rays to be specularly reflected from the facet bottom, and derive expressions for the mean and variance of incoherent intensity at a point receiver for a transmitted cw signal. The results are sufficiently general to permit their use with different bottom-acoustic models, but we employ Mackenzie theory here. Relative effects of structure and topography are compared. Subsequently, small-scale roughness is superimposed on the facets, and the added consequences of scattering are considered.

Random-bottom Structural and Topographical Effects on Sound Transmission in a Shallow Channel

by

W. L. Siegmann, M. J. Jacobson, and C. E. Ashley

Department of Mathematical Sciences

Rensselaer Polytechnic Institute

Troy, New York 12180-3590

RPI Math. Rep. No. 158

May 30, 1986

This work was sponsored by

Code 1125UA, Office of Naval Research

Contract No. N00014-86-K-0129

NR 4254007

ABSTRACT

Effects of horizontal stochastic bottom structure on acoustic intensity in an isospeed ocean have been studied previously by the authors [J. Acoust. Soc. Am. 76, 1445-1455 (1984)]. The bottom density and sound speed were taken to be random and ray theory was used. In this study we add a rough water-bottom interface, consisting of large-scale, two dimensional random facets upon which small-scale roughness may be superimposed. Each facet is assumed to possess small random depth deviation, slope, and curvature. Initially, we take acoustic rays to be specularly reflected from the facet bottom, and derive expressions for the mean and variance of incoherent intensity at a point receiver for a transmitted cw signal. The results are sufficiently general to permit their use with different bottom-acoustic models, but we employ Mackenzie theory here. Relative effects of structure and topography are compared. Subsequently, small-scale roughness is superimposed on the facets, and the added consequences of scattering are considered.

INTRODUCTION

Acoustical consequences of bottom characteristics are well known to be particularly important in shallow water, because of the extensive interaction between sound waves and the bottom. This complication is compounded by geological processes causing sedimentation in shallow water, so that there is usually a larger degree of lateral variability in bottom composition than in the deep ocean.[1]

Effects of bottom topography on acoustic signals have been studied extensively (e.g., Ref. 2). The influence on sound propagation of horizontal ocean bottom structure, which is regarded as being characterized by its density and sound speed, has also received attention (e.g., Ref. 3). A few investigations have discussed the situation when both types of bottom variations are assumed present.[4,5] However, none of which we are aware has studied their relative effects, or has used the statistical methods presented here. Since structural and topographical properties are typically not well known, it is appropriate to model them in a statistically random fashion.

In this paper, we use the ray theory of propagation, and the vertical plane containing the point source and receiver is taken normal to a two-dimensional rough bottom. The acoustic field at a point receiver is composed of individual ray arrivals which are transmitted from an omnidirectional cw source. In much of this study, ray paths between the source and receiver are determined by specular reflection from a bottom with large-scale roughness and from a horizontal ocean surface. Hence, all rays are coplanar. Because we are assuming an ocean of shallow depth, the water is taken to have constant sound speed and density. Our primary objective is to determine statistics of incoherent intensity at a receiver in terms of statistics of the bottom structure and topography.

In an earlier paper by us,[3] the influence of horizontal structural variations alone on acoustic propagation was investigated. We use similar methods here, and assume the bottom has small random variations in sound speed and density in the horizontal direction. We generalize our previous investigation by permitting a rough water-bottom interface. At first, we consider a bottom composed of a collection of large-scale facets. Other studies have used such a facet-bottom model to include roughness effects.[6,7] Our facets are characterized in part by the locations of bottom-reflection points of an "ideal" ray from a horizontal bottom. Each facet is assumed to have a small random inclination angle and depth deviation. In addition, each facet has curvature and the radius of curvature is taken to be large with respect to acoustic wavelength. Consequently, the curvature of each is modeled as a random variable with small magnitude. Subsequently, small-scale roughness is added to the facets.

In Sec. I, we present expressions for bottom loss and spreading loss, approximating both by truncated Maclaurin series. In Sec. II, expressions for mean incoherent intensity and its variance are developed. Mackenzie bottom loss and reasonable correlation functions for our bottom random variables are incorporated into our equations. Section III presents, and provides discussion of, numerical results obtained from the model in Sec. II. In Sec. IV, we superimpose microroughness onto our random facets, and examine their consequences on intensity. A summary of principal results appears in Sec. V.

I. BASIC FORMULATION

Using the notation of Ref. 3, we consider an isospeed sound channel of mean depth H. The xy-plane contains a point source S at $(0,h_S)$ and a receiving point R at (R,h_R). In Fig. 1 an "ideal" ray $\bar{r}_{nj}$ appears as the dashed

curve. This ray has initial angle $\bar{\theta}_{oj}^{(n)}$ at the source, the same angle magnitude at the receiver and at each bottom reflection. As indicated in Fig.1, all angles are measured positive clockwise from the positive x-direction. The index j can take on integer values from 1 to 4, depending on the orientation of the ray at the source and receiver. In Fig. 1, j has the value one, which corresponds to a ray with downward direction at the source and upward direction at the receiver. The ray $\bar{r}_{nj}$ intercepts the mean bottom n times at the points $(\bar{x}_{ij}^{(n)}, H)$, i = 1, ..., n.

Also shown in Fig. 1 is the corresponding "actual" ray r_{nj}, which appears as the solid curve. The initial angle of this ray is denoted by $\theta_{oj}^{(n)}$. It intercepts the two-dimensional water-bottom interface n times at the points $(x_{ij}^{(n)}, y_{ij}^{(n)})$, i = 1, ..., n. It can be shown that, for a bottom that deviates only slightly from y = H, there is an actual ray r_{nj} corresponding to each ideal ray $\bar{r}_{nj}$ for each ordered pair (n,j).

The tangent line to the bottom at the point $(x_{ij}^{(n)}, y_{ij}^{(n)})$ intercepts the line $x = \bar{x}_{ij}^{(n)}$ at a depth that differs from H by the signed quantity $\mathcal{D}_{ij}^{(n)}$. Thus, $\mathcal{D}_{ij}^{(n)}$ is one measure of the depth deviation of a bottom facet. It is positive (or negative) when the facet depth is greater (or less) than H at $\bar{x}_{ij}^{(n)}$. We denote the small inclination angle of the tangent line to the bottom at $(x_{ij}^{(n)}, y_{ij}^{(n)})$ by $a_{ij}^{(n)}$ and the incident angle r_{nj} (i.e., the angle the incident ray makes with the x-direction at the bottom reflection) by $\theta_{ij}^{(n)}$. When the bottom facet in the neighborhood of the point of reflection is concave down, as is the case shown in Fig. 1, we take the "signed curvature" $\kappa_{ij}^{(n)}$ to be positive, and when it is concave up, $\kappa_{ij}^{(n)}$ is negative. Thus, at $(x_{ij}^{(n)}, y_{ij}^{(n)})$ the bottom has a radius of curvature $\ell_{ij}^{(n)} = 1/|\kappa_{ij}^{(n)}|$. Hereafter, a primed length quantity denotes its normalization with respect to the mean depth H

(e.g., $h_s' = h_s/H$). We consider $a_{ij}^{(n)}$, $\mathcal{D}_{ij}^{(n)'}$, and $\kappa_{ij}^{(n)'} = H\kappa_{ij}^{(n)}$ to be random variables of the bottom topography with small magnitudes.

The grazing angle $\psi_{ij}^{(n)}$ of ray r_{nj} is the angle between the incident ray and the tangent line to the bottom at $(x_{ij}^{(n)}, y_{ij}^{(n)})$, assuming specular reflection. This angle is measured positive clockwise from a tangent line to the bottom in the ray direction. The grazing angle can be written in terms of a Maclaurin series in powers of $a_{ij}^{(n)}$ and $\mathcal{D}_{ij}^{(n)'}$. This series, truncated after linear terms in these variables, is given by

$$\psi_{ij}^{(n)} = -\nu\,\bar{\theta}_{oj}^{(n)} + \mu_{ij}^{(n)} , \tag{1}$$

where

$$\mu_{ij}^{(n)} = 2\sum_{\ell=1}^{n}\left\{\frac{1}{\bar{u}_{nj}}\left[2(n-\ell) + 1 - \lambda h_R'\right] a_{\ell j}^{(n)} + \frac{R'}{(R'^2 + \bar{u}_{nj}^2)}\,\mathcal{D}_{ij}^{(n)'}\right\} - 2\sum_{\ell=1}^{i-1} a_{\ell j}^{(n)} - a_{ij}^{(n)} . \tag{2}$$

In Eq. (2), $\bar{u}_{nj}'$ is the normalized version of the total vertical distance $\bar{u}_{nj}$ traveled by the mean ray r_{nj}, where

$$\bar{u}_{nj} = 2n\,H + \nu\,h_s - \lambda\,h_r . \tag{3}$$

The symbols ν and λ are parameters defined by

$$\nu = (-1)^j \tag{4}$$

and

$$\lambda = (2.5 - j)/|2.5-j| . \tag{5}$$

We turn next to our model for the structure of the bottom. We consider variations in the horizontal xy-plane, both in the bottom density $\rho_{ij}^{(n)}$ and sound speed $c_{ij}^{(n)}$ at the ith bounce of ray r_{nj}. We write

$$\rho_{ij}^{(n)}/\rho_1 = (\rho_2/\rho_1)(1 + \varepsilon_{ij}^{(n)}) , \tag{6}$$

where ρ_2 is the constant horizontally - averaged density of the bottom, ρ_1 is the constant water density, and $\varepsilon_{ij}^{(n)}$ is a small random quantity. Similarly,

$$c_1/c_{ij}^{(n)} = (c_1/c_2)(1 + \delta_{ij}^{(n)}) , \tag{7}$$

where c_1 and c_2 are the constant water sound speed and the mean bottom sound speed. The quantity $\delta_{ij}^{(n)}$ is another small random variable. As discussed in Ref. 3, it is possible to approximately relate c_2 and $\delta_{ij}^{(n)}$ to ρ_2 and $\varepsilon_{ij}^{(n)}$, respectively, by the equations

$$c_2(\rho_2) = 2270.9 - 1194.4\rho_2 + 474.6\rho_2^2 \tag{8a}$$

and

$$\varepsilon_{ij}^{(n)} = -2\,\delta_{ij}^{(n)} . \tag{8b}$$

For convenience in the expansions to follow, we assume that the three topographical random variables, $\mathcal{D}_{ij}^{(n)'}$, $a_{ij}^{(n)}$, and $\kappa_{ij}^{(n)'}$, and the two structural random variables, $\varepsilon_{ij}^{(n)}$ and $\delta_{ij}^{(n)}$, are of the same small order of magnitude. This enables us to keep terms of like degree in all variables. Different orders can, of course, be assumed, so long as all expansions are performed with consistency.

The sound source S emits a unity - amplitude cw signal, which arrives at the receiver R along ray r_{nj} with amplitude a_{nj}. For the large-scale facet bottom, the received amplitude is taken to differ from unity because of geometrical spreading loss and bottom loss. Other losses could be included, but will not be considered here. We may write

$$a_{nj} = \Lambda_{nj}^{-1/2}\, \mathcal{B}_{nj} , \tag{9}$$

where Λ_{nj} is the spreading loss and $\mathcal{B}_{nj}$ is the total bottom loss. In Ref. 8, a spreading loss equation is derived for rays specularly reflected from a bottom composed of large-scale curved facets. Truncated to linear terms,

it is

$$\Lambda_{nj} = H^2\{(R'^2 + \bar{u}'^2_{nj}) + 2\sum_{i=1}^{n}[2\bar{u}'_{nj}\,\mathcal{D}'^{(n)}_{ij} + \frac{(R'^2 + \bar{u}'^2_{nj})}{\bar{u}'_{nj}}\,\Omega^{(n)}_{ij}\,\kappa'^{(n)}_{ij}]\}\ , \qquad (10)$$

where $\Omega^{(n)}_{ij}$ is given by

$$\Omega^{(n)}_{ij} = (R'^2/\bar{u}'^2_{nj} + 1)\,[-4i^2 + 2(2n + 2 - \lambda h'_R - \nu h'_s)i - (1 - \nu h'_s) \times (2n + 1 - \lambda h'_R)]\ . \qquad (11)$$

This formula is valid if n is not too large. Note that, to first order, the slopes $a^{(n)}_{ij}$ of the facets do not contribute to Λ_{nj}. For any particular ray r_{nj}, the effects of the depth deviations $\mathcal{D}'^{(n)}_{ij}$ are the same for each bottom reflection because the term multiplying $\mathcal{D}'^{(n)}_{ij}$ is independent of i. However, the random variables $\kappa'^{(n)}_{ij}$ are weighted according to which bottom is considered; the curvature of bottom facets near midrange has the greatest effect, and that near the source and receiver has the least influence.

In Eq. (9), the decrease $\mathcal{B}_{nj}$ in amplitude due to all the bottom losses of ray r_{nj} is

$$\mathcal{B}_{nj} = \prod_{i=1}^{n} \mathcal{B}^{(n)}_{nj}\ , \qquad (12)$$

where $\mathcal{B}^{(n)}_{ij}$ is the reflection coefficient of r_{nj} at its i^{th} bottom bounce. We assume that the coefficient $\mathcal{B}^{(n)}_{ij}$ depends on both grazing angle and bottom structural properties. It is then possible to expand $\mathcal{B}^{(n)}_{ij}$ in a Maclaurin series with respect to the random variations of these quantities. To first-order terms, there is then an expression with the form

$$\mathcal{B}^{(n)}_{ij} = A_{nj} + B_{nj}\varepsilon^{(n)}_{ij} + C_{nj}\delta^{(n)}_{nj} + D_{nj}\mu^{(n)}_{ij}\ , \qquad (13)$$

where $\mu^{(n)}_{ij}$ is given by Eq. (2). The coefficients of the random variables in Eq. (13) depend on the reflection theory used and the mean bottom values

selected.

II. INTENSITY MOMENTS

We consider two measures of the sound field at the receiver. These are the mean and variance of the incoherent intensity I, given by

$$I = \sum_{n=0}^{N} \sum_{j=1}^{4} a_{nj}^2 \ . \tag{14}$$

Because the losses experienced by successive ray arrivals grow rapidly, we need consider only those rays experiencing some number N or fewer bottom reflections. Specifically, we elect to neglect ray arrivals which have amplitudes less than 1% of the arrival with largest amplitude.

We wish to determine expressions for the mean and variance of I,

$$\mu(I) = E(I) \tag{15}$$

and

$$\sigma^2(I) = E(I^2) - E^2(I) \ , \tag{16}$$

where E denotes expectation and I is a function of the five types of random variables introduced in Sec. I. We assume that the mean of each type is zero,

$$E(\varepsilon_{ij}^{(n)}) = E(\delta_{ij}^{(n)}) = E(\mathcal{D}_{ij}^{(n)'}) = E(a_{ij}^{(n)}) = E(\kappa_{ij}^{(n)'}) = 0 \ , \tag{17}$$

and that each type has a constant standard deviation,

$$\sigma(\varepsilon_{ij}^{(n)}) = \sigma_{\varepsilon} \ , \tag{18a}$$

$$\sigma(\delta_{ij}^{(n)}) = \sigma_{\delta} \ , \tag{18b}$$

$$\sigma(\mathcal{D}_{ij}^{(n)'}) = \sigma_{\mathcal{D}'} \tag{18c}$$

$$\sigma(a_{ij}^{(n)}) = \sigma_{a} \ , \tag{18d}$$

and

$$\sigma(\kappa_{ij}^{(n)'}) = \sigma_{\kappa'} \ . \tag{18e}$$

We also assume that any two different topographical variables are uncorrelated, and that topographical and structural random variables are not correlated. For example, the concavity at a bottom reflection is taken to be uncorrelated with both the depth deviation and the density there. However, we do allow each random variable to be correlated with itself at two separate bottom reflections. Thus,

$$E(\varepsilon_{ij}^{(n)}\ \varepsilon_{\ell k}^{(m)}) = \sigma_\varepsilon^2\ C_\varepsilon(\varepsilon_{ij}^{(n)},\ \varepsilon_{\ell k}^{(m)})\ , \tag{19a}$$

$$E(\delta_{ij}^{(n)}\ \delta_{\ell k}^{(m)}) = \sigma_\delta^2\ C_\delta(\delta_{ij}^{(n)},\ \delta_{\ell k}^{(m)})\ , \tag{19b}$$

$$E(\mathcal{D}_{ij}^{(n)'}\ \mathcal{D}_{\ell k}^{(m)'}) = \sigma_{\mathcal{D}'}^2\ C_{\mathcal{D}'}(\mathcal{D}_{ij}^{(n)'},\ \mathcal{D}_{\ell k}^{(m)'})\ , \tag{19c}$$

$$E(a_{ij}^{(n)}\ a_{\ell k}^{(m)}) = \sigma_a^2\ C_a(a_{ij}^{(n)},\ a_{\ell k}^{(m)})\ , \tag{19d}$$

and

$$E(\kappa_{ij}^{(n)'}\ \kappa_{\ell k}^{(m)'}) = \sigma_{\kappa'}^2\ C_{\kappa'}(\kappa_{ij}^{(n)'},\ \kappa_{\ell k}^{(m)'})\ . \tag{19e}$$

In Eqs. (19), any function $C(a,b)$ represents the correlation coefficient of the random quantities a and b. Also, the structural random variables $\varepsilon_{ij}^{(n)}$ and $\delta_{ij}^{(n)}$ are correlated as in Ref. 3, so that

$$E(\varepsilon_{ij}^{(n)}\ \delta_{\ell k}^{(m)}) = \sigma_\varepsilon \sigma_\delta\ C_{\varepsilon\delta}(\varepsilon_{ij}^{(n)},\ \delta_{\ell k}^{(m)})\ . \tag{19f}$$

Using the particular relationship given by Eq. (8b), we may write

$$\sigma_\delta^2\ C_\delta(\delta_{ij}^{(n)},\ \delta_{\ell k}^{(m)}) = 1/4\ \sigma_\varepsilon^2\ C_\varepsilon(\varepsilon_{ij}^{(n)},\ \varepsilon_{\ell k}^{(m)})\ , \tag{20a}$$

and

$$\sigma_\varepsilon \sigma_\delta\ C_{\varepsilon\delta}(\varepsilon_{ij}^{(n)},\ \delta_{\ell k}^{(m)}) = -1/2\ \sigma_\varepsilon^2\ C_\varepsilon(\varepsilon_{ij}^{(n)},\ \varepsilon_{\ell k}^{(m)})\ , \tag{20b}$$

so that we have only one correlation function C_ε for the structure.

It is now possible to determine $\mu(I)$ and $\sigma^2(I)$. Keeping through first-order terms in the random variables for the mean, we have

$$\mu(I) = \sum_{n=0}^{N} \sum_{j=1}^{4} A_{nj}^{2n} / [H^2 (R'^2 + \bar{u}_{nj}'^2)] \ . \tag{21}$$

In Eq. (21), A_{nj} and $H^2(R'^2 + \bar{u}_{nj}'^2)$ represent the leading-order terms of the bottom loss and spreading loss, respectively (see Eqs. (13) and (10)). No first-order terms appear in Eq. (21) due to the assumptions of Eq. (17). We keep through second-order terms in the variance so that the standard deviation is correct to first order. Therefore, for the variance, we obtain an expression of the form

$$\sigma^2(I) = V_\varepsilon \sigma_\varepsilon^2 + V_{\mathcal{D}'} \sigma_{\mathcal{D}'}^2 + V_a \sigma_a^2 + V_{\kappa'} \sigma_{\kappa'}^2 \ . \tag{22}$$

The quantities $V_\varepsilon \sigma_\varepsilon^2$, $V_{\mathcal{D}'} \sigma_{\mathcal{D}'}^2$, $V_a \sigma_a^2$, and $V_{\kappa'} \sigma_{\kappa'}^2$ in Eq. (22) represent symbolically the contributions to the variance from the bottom structure, depth deviation, slope, and curvature. After much manipulation, the coefficients can be found as the following formulas:

$$V_\varepsilon = \frac{4}{H^4} \sum_{n=1}^{N} \sum_{m=1}^{N} \sum_{j=1}^{4} \sum_{k=1}^{4} \frac{A_{nj}^{2n-1} A_{mk}^{2m-1}}{(R'^2 + \bar{u}_{nj}'^2)(R'^2 + \bar{u}_{mk}'^2)} \left[B_{nj} B_{mk} - B_{nj} C_{mk} + \frac{1}{4} C_{nj} C_{mk} \right] \sum_{i=1}^{n} \sum_{\ell=1}^{m} C_\varepsilon (\varepsilon_{ij}^{(n)}, \varepsilon_{\ell k}^{(m)}) \ , \tag{23a}$$

$$V_{\mathcal{D}'} = \frac{16}{H^4} \sum_{n=1}^{N} \sum_{m=1}^{N} \sum_{j=1}^{4} \sum_{k=1}^{4} \frac{A_{nj}^{2n} A_{mk}^{2m}}{(R'^2 + \bar{u}_{nj}'^2)^2 (R'^2 + \bar{u}_{nj}'^2)^2} \left(\frac{R' D_{nj}^{\ n}}{A_{nj}} - \bar{u}_{nj}' \right) \times \left(\frac{R' D_{mk}^{\ m}}{A_{mk}} - \bar{u}_{mk}' \right) \sum_{i=1}^{n} \sum_{\ell=1}^{m} C_{\mathcal{D}'} (\mathcal{D}_{ij}^{(n)'}, \mathcal{D}_{\ell k}^{(m)'}) \ , \tag{23b}$$

$$V_a = \frac{4}{H^4} \sum_{n=1}^{N} \sum_{m=1}^{N} \sum_{j=1}^{4} \sum_{k=1}^{4} \frac{A_{nj}^{2n-1} A_{mk}^{2m-1} D_{nj} D_{mk}}{\bar{u}_{nj}' \bar{u}_{mk}' (R'^2 + \bar{u}_{nj}'^2)(R'^2 + \bar{u}_{mk}'^2)} \sum_{i=1}^{n} \sum_{\ell=1}^{m} \{[2(n-i) + 1]\nu h_s' + (2i-1)\lambda h_r'\} \{[2(m-\ell) + 1]\nu h_s' + (2\ell-1)\lambda h_r'\} C_a (a_{ij}^{(n)}, a_{\ell k}^{(m)}) \ , \tag{23c}$$

and

$$V_{\kappa'} = \frac{4}{H^4} \sum_{n=1}^{N} \sum_{m=1}^{N} \sum_{j=1}^{4} \sum_{k=1}^{4} \frac{A_{nj}^{2n} A_{mk}^{2m}}{\overline{u'}_{nj} \overline{u'}_{mk} (R'^2 + \overline{u'}_{nj}^2)(R'^2 + \overline{u'}_{mk}^2)}$$

$$\times \sum_{i=1}^{n} \sum_{\ell=1}^{m} \Omega_{ij}^{(n)} \Omega_{\ell k}^{(m)} C_{\kappa'}(\kappa_{ij}^{(n)'} \kappa_{\ell k}^{(m)'}) \, . \tag{23d}$$

Note that the variance depends only on the first-order coefficients B_{nj}, C_{nj}, and D_{nj} of the random variables in Eq. (13), and not on any second-order coefficients. That is, even if the coefficients of second-order terms were somehow known in Eq. (13), these would not appear in Eqs. (22) and (23), due to the averaging process.

Investigation of Eqs. (21) and (22) for the mean and variance of intensity requires specification of a bottom reflection model. We choose here to use Mackenzie's model,[9] in which the reflection coefficient is given by

$$\mathcal{B}_{ij}^{(n)} = [(h_+ - \sigma \sin \psi_{ij}^{(n)})^2 + h_-^2]^{1/2} \times [(h_+ + \sigma \sin \psi_{ij}^{(n)})^2 + h_-^2]^{-1/2} \, , \tag{24a}$$

where

$$h_\pm = \{\pm g + [(\alpha/\beta)^2 + g^2]^{1/2}\}^{1/2} \, , \tag{24b}$$

$$g = \frac{1}{2} [1 - (v_2/c_1)^2 \cos^2 \psi_{ij}^{(n)} - (\alpha/\beta)^2] \, , \tag{24c}$$

and

$$\sigma = \rho_{ij}^{(n)} v_2/\rho_1 c_1 \, . \tag{24d}$$

The quantity σ is the impedance and v_2 is the phase speed of acoustic waves in the bottom and, to an excellent approximation, is given by $v_2 \doteq c_{ij}^{(n)}$. The quantity α/β is the ratio of the imaginary to real parts of the wave number of acoustic waves in the bottom. This term provides a dissipative mechanism for

sound which enters the bottom. In Ref. 3 it is explained how values for α/β are determined from formulas derived by Hamilton.[10]

Using Mackenzie theory, we obtain expressions for the coefficients A_{nj}, B_{nj}, C_{nj}, and D_{nj} which appear in Eq. (13). They are calculated to be

$$A_{nj} = M^{-}_{nj}/M^{+}_{nj} , \tag{25a}$$

$$B_{nj} = Q_{nj}\,(S_{nj} - P_{nj})/[(M^{+}_{nj})^3 M^{-}_{n}] , \tag{25b}$$

$$C_{nj} = Q_{nj}\,\bar{c}^2\,(P_{nj} + S_{nj} - 4T_{nj}) + Q_{nj}\,(S_{nj} - P_{nj}) \times [P_{nj}(M^{+}_{nj})^3(M^{-}_{nj})]^{-1} \cos^2 \bar{\theta}^{(n)}_{oj} , \tag{25c}$$

and

$$D_{nj} = R'Q_{nj}[S_{nj}(1 - 1/\bar{\rho}^2) - P_{nj} + (S^2_{nj}/\bar{\rho}^2 + 4T_{nj}\bar{c}\,\sin|\bar{\theta}^{(n)}_{nj}|)/P_{nj}] \times [\bar{u}'_{nj}(M^{+}_{nj})^3 M^{-}_{nj}]^{-1} , \tag{25d}$$

where

$$M^{\pm}_{nj} = [P_{nj} \pm Q_{nj} + S_{nj}]^{1/2} , \tag{25e}$$

$$P_{nj} = 2\,(\alpha^2/\beta^2 + T_{nj}{}^2)^{1/2} , \tag{25f}$$

$$Q_{nj} = 2\sigma\,[T_{nj} + (\alpha^2/\beta^2 + T_{nj}{}^2)^{1/2}]^{1/2} \sin|\bar{\theta}^{(n)}_{oj}| , \tag{25g}$$

$$S_{nj} = \bar{\sigma}^2 \sin^2 \bar{\theta}^{(n)}_{oj} , \tag{25h}$$

$$T_{nj} = \frac{1}{2}\,[1 - \bar{c}^2 \cos \bar{\theta}^{(n)}_{oj} - \alpha^2/\beta^2] , \tag{25i}$$

$$\bar{\sigma} = \bar{c}\,\bar{\rho} , \tag{25j}$$

$$\bar{c} = c_2/c_1 , \tag{25k}$$

and

$$\bar{\rho} = \rho_2/\rho_1 . \tag{25ℓ}$$

The above formulas reduce to those in Ref. 3 where the bottom was horizontal. The notation has been changed slightly, however.

To evaluate the intensity variance in Eq. (22), we also need to specify correlation coefficients for the random variables. We choose the Gaussian forms

$$C_\varepsilon(\varepsilon_{ij}^{(n)}, \varepsilon_{\ell k}^{(m)}) = \exp\left[-(x_{ij}^{(n)} - x_{\ell k}^{(m)})^2/L_\varepsilon^2\right], \tag{26a}$$

$$C_{\mathcal{D}'}(\mathcal{D}_{ij}^{(n)'}, \mathcal{D}_{\ell k}^{(m)'}) = \exp\left[-(x_{ij}^{(n)} - x_{\ell k}^{(m)})^2/L_{\mathcal{D}'}^2\right], \tag{26b}$$

$$C_a(a_{ij}^{(n)}, a_{\ell k}^{(m)}) = \exp\left[-(x_{ij}^{(n)} - x_{\ell k}^{(m)})^2/L_a^2\right], \tag{26c}$$

and

$$C_{\kappa'}(\kappa_{ij}^{(n)'}, \kappa_{\ell k}^{(m)'}) = \exp\left[-(x_{ij}^{(n)} - x_{\ell k}^{(m)})^2/L_{\kappa'}^2\right], \tag{26d}$$

Here, $|x_{ij}^{(n)} - x_{\ell k}^{(m)}|$ is the horizontal distance between the i^{th} bottom reflection of ray r_{nj} and the ℓ th bottom bounce of ray r_{mk}. The parameters L_ε, $L_{\mathcal{D}'}$, L_a, $L_{\kappa'}$ are the correlation lengths associated with each random variable, and each represents the value of $|x_{ij}^{(n)} - x_{\ell k}^{(m)}|$ where C takes the value 1/e. The correlation function for the bottom sound speed variation $\delta_{ij}^{(n)}$ is related to C_ε by Eqs. (20). Of course, other forms for the correlation functions could be used, if desired or if suggested by bottom observations.

III. NUMERICAL RESULTS

We now investigate the behavior of the mean and variance of the received incoherent intensity, Eqs. (21) and (22), respectively. We incorporate expressions from Eqs. (23) into the variance and use the Mackenzie bottom model formulas, Eqs. (24) and (25), for the coefficients of bottom loss and spreading loss. For the correlation coefficients in the variance, we use the Gaussian forms shown in Eqs. (26). As indicated in the theoretical development, our expressions apply to relatively large-scale topographical variations.

Graphs of the moment ratio

$$M_R = 10 \log_{10} \mu(I)/\sigma(I) \tag{27}$$

will appear in our figures. This is, in effect, a signal-to-noise ratio in dB. Small (i.e., large negative) values for M_R mean that the fluctuation in intensity is large relative to its mean. Conversely, large (positive) values correspond to the standard deviation being small compared to the mean, i.e. a stronger "signal."

For convenience in our numerical calculations, we place the source and receiver on the ocean surface. Of course, other configurations could be used without difficulty, if desired. The density and sound-speed values in the water are taken to be $\rho_1 = 1.025$ g/cm^3 and $c_1 = 1523$ m/s. We found, for the parameter values chosen, that a maximum number N of at most 7 bottom reflections needed to be included for any aspect ratio R', according to the criterion presented in Sec. II. Rays with a greater number of bottom reflections were shown to negligibly affect the results. From Eq. (23c), it is apparent that for source and receiver on the surface ($h_s' = h_r' = 0$), the contribution from the bottom slope vanishes because $V_a = 0$. From numerical calculations for other source and receiver locations, we found that the contributions from the bottom slope terms is always insignificant compared to the structural and curvature contributions. The quantity $V_{\mathcal{D}'}$ can also be demonstrated to be relatively small compared to V_ε and $V_{\kappa'}$.

Figure 2 shows moment ratio, Eq. (27), versus mean bottom density ρ_2. The values used for ρ_2 are typical of bottoms on the continental shelf. Based on data from various sources,[11] we have chosen the values of the standard deviations for our random variables to be 0.1 (for σ_δ, $\sigma_{\mathcal{D}'}$, and $\sigma_{\kappa'}$) and 0.2 (for σ_ε). These are consistent with our earlier assumption that the random

variables are of the same order of magnitude and with Eq. (8b). We have kept the aspect ratio constant (R' = 20) in this figure, and each curve corresponds to different values of the two normalized (with respect to H) correlation lengths L'_ε and $L'_{\kappa'}$. Also, we have taken the correlation lengths of the two topographical random variables, $L_{\mathcal{D}'}$ and $L_{\kappa'}$, to be equal.

In the figure, L'_ε and $L'_{\kappa'}$, take on values of zero and infinity. When $L'_{\kappa'}$ is near zero, it means there is little correlation between bottom topography at any two given points. On the other hand, when $L'_{\kappa'}$ is very large, the topography is correlated even at widely separated bottom locations. Similar statements apply for the normalized correlation length of bottom structure, L'_ε. It is apparent from Fig. 2 that varying the normalized topographical correlation length $L'_{\kappa'}$ has a much greater effect on M_R than varying L'_ε. For example, at ρ_2 = 2.1 g/cm^3, when $L'_{\kappa'}$ increases from zero to infinity, there is about a 4 dB change in M_R. In contrast, varying L'_ε has very little effect. The quantity L'_ε has some influence only when the mean bottom density is small. Indeed, this is where the Mackenzie reflection coefficient tends to vary most rapidly with changes in bottom density or sound speed. However, at no ρ_2 value does varying L'_ε cause more than a 1 dB change in M_R. This figure suggests that the moment ratio is insensitive to the precise value of the horizontal correlation length for density or sound-speed variations.

When the normalized correlation length $L'_{\kappa'}$ in Eq. (26d) increases, the correlation coefficient $C_{\kappa'}$ increases as well. Thus, for small $L'_{\kappa'}$, the correlation between the bottom concavity at two points is small, and the fluctuations in concavity at these points tend to cancel. Consequently, $\sigma(I)$ decreases, causing the moment ratio to increase as $L'_{\kappa'}$ decreases. For larger $L'_{\kappa'}$, there is more of a relationship between the concavities at two bottom points. The reduction in fluctuations will not be as great as for small $L'_{\kappa'}$.

Hence, $\sigma(I)$ grows as $L'_{\kappa'}$ increases and, therefore, M_R decreases. The same type of argument applies for any of the other random variables and their corresponding correlation lengths. However, as suggested by Fig. 2, it is the variations of $L'_{\kappa'}$ which have the largest effects on our model. With this picture of the effects of different values for correlation lengths, we proceed to investigate the influence of other parameters. In all subsequent figures of this paper, we will take all correlation lengths as approximately zero.

Figure 3 illustrates the behavior of the moment ratio versus mean bottom density for three values of the aspect ratio R'. For a given value of R', we observe a general upward trend in M_R as ρ_2 increases. This same trend can be seen in Fig. 2, of course. For low-density bottoms, the Mackenzie reflection coefficient tends to fluctuate more as ρ_2 varies than for larger ρ_2. This causes $\sigma(I)$ to be large, so that M_R in dB becomes more negative. For example, when R' = 5, there is approximately 8 dB difference between the values of M_R at $\rho_2 = 1.5$ g/cm^3 and $\rho_2 = 2.1$ g/cm^3. It might be anticipated that the variance of the intensity would become smaller as R' decreased and thus that M_R would increase. This is true for high-density bottoms, but not for lower values of ρ_2. At $\rho_2 = 1.6$ g/cm^3, for example, M_R is larger for R' = 10 than for R' = 5. As was stated in Ref. 3, low-density bottoms have a less well-defined behavior as compared to higher density ones.

In Fig. 4, we show the relative effects on moment ratio of random bottom structure, random bottom topography, and a combination of both features. The quantity M_R is plotted against the aspect ratio, with ρ_2 held constant at 1.8 g/cm^3. The heavy solid curve represents the combined effects of topography and structure on moment ratio (i.e., all standard deviations in Eq. (22) are non-zero). The dashed curve corresponds to a horizontal bottom with random structure (i.e., $\sigma_{D'} = \sigma_a = \sigma_{\kappa'} = 0$ in Eq. (22)). Similarly, the light solid

curve corresponds to a structurally homogeneous bottom with random topography (i.e., $\sigma_\varepsilon = 0$ in Eq. (22)). The relatively large (i.e., small negative) values M_R on the heavy solid curve for small R' indicate relatively small intensity fluctuations. On the other hand, the small (i.e., large negative) values of M_R for large R' correspond to large variations of the intensity about its mean. This same trend will be seen in Figs. 5 and 7.

It is also apparent in Fig. 4 that for small aspect ratios (approximately $R' < 5$), the random bottom structure makes a greater contribution to M_R than does the random bottom roughness. For larger ratios, however, the opposite is true. The dashed curve, corresponding to a horizontal bottom with random structure only, tends to oscillate. This is due to the large variability in the bottom reflection coefficient with grazing angle. The light solid curve, which corresponds to a structurally homogeneous bottom with roughness, is dominated by curvature effects. Because the bottom reflection coefficient does not depend on the interface curvature, this curve monotonically decreases with increasing R'. The bottom curvature tends to focus and defocus ray bundles through the spreading loss contribution. This causes $\sigma(I)$ to be greater, and the effect increases as the grazing angle decreases, i.e., as R' increases.

Figure 5 is a graph which can be compared with Fig. 4. The mean bottom density is decreased from $\rho_2 = 1.8$ g/cm^3 (e.g., fine sand) in Fig. 4 to $\rho_2 = 1.6$ g/cm^3 (e.g., silty clay) in Fig. 5. The general shapes of the corresponding curves in each figure are broadly similar. However, in the curves of Fig. 5, the moment ratio becomes more negative. This is due to the influence of the random structure, not to that of the topography. As we discussed in connection with Fig. 3, a lower-density bottom usually results in a larger value for $\sigma(I)$. The smaller mean density value used for Fig. 5 also has the effect of lengthening the interval on the R' axis in which structure contributes more to M_R than

topography. This interval extends to about R' = 9 in Fig. 5, compared with about R' = 5 in Fig. 4.

A three-dimensional graph is shown in Fig. 6, in which we have varied the standard deviations of the two dominant random variables, σ_ε and $\sigma_{\kappa'}$. This perspective figure shows how these quantities influence the moment ratio. The aspect ratio and mean bottom density are held constant at 10 and 1.8 g/cm^3. Each of the standard deviations is varied from 0 to 0.2. When $\sigma_{\kappa'}$ is near zero, increasing σ_ε has the effect of decreasing M_R. As $\sigma_{\kappa'}$ becomes closer to 0.2 however, varying σ_ε has little effect on M_R. For a constant value of σ_ε, increasing $\sigma_{\kappa'}$ always causes a decrease in M_R. These types of behavior occur because at R' = 10, the topography of the bottom has a larger influence on the intensity variance than does the structure. If R' were chosen, for example, to be less than five, then varying σ_ε would have a greater effect than changing $\sigma_{\kappa'}$, because then structure dominates over topography. This was seen previously in Fig. 4.

Figure 7 illustrates how the aspect ratio R' and mean bottom density ρ_2 affect moment ratio. In fact, Figs. 3, 4, and 5 are cross-sections of Fig. 7, but were introduced first because of their greater ease of interpretation. For a given density, the dominant n = 1 (one reflection) ray has a specific R' value, or grazing-angle value, at which the Mackenzie reflection coefficient drops from a value near one to a much lower value. This occurs near the critical angle of Rayleigh reflection theory.[12] In turn, a large $\sigma(I)$ value is produced, and hence, a large negative value for M_R. The indentation in the surface of Fig. 7 is the general consequence of this feature. As ρ_2 increases, the value of R' at which this effect occurs decreases, since the grazing angle increases. For rays with n > 1, the same effect occurs, but these rays are attenuated by each bottom reflection and, consequently, do not have so

large an influence on received intensity. It can also be seen from Fig. 7 that, for any ρ_2 value, the moment ratio experiences an overall decrease as R' increases form 1 to 20. This decrease is most dramatic for lower density bottoms.

IV. SMALL-SCALE ROUGHNESS

In previous sections, we assumed specular reflection from a facet bottom, implying facet lengths which are large in acoustic wave-wengths. In this section, we enhance our bottom model by superimposing small-scale roughness on the facets. It is not uncommon for ocean bottoms to be modeled using two degrees of roughness.[13-16]

Eckart[17] gave a Kirchhoff solution for the acoustic signal reflected by a rough surface which was later modified by Clay.[18] We use Clay's method here to describe the sound scattered by the small-scale roughness. A more general approach, which reduces to Clay's results, is given by Kuperman.[19]

We assume that the dimensions of the scattering area are much greater than the acoustic wavelength λ, and these dimensions are in turn much less than the distance to the source or to the receiver. Let $y = \zeta_{ij}^{(n)}(x)$ be the deviation of the irregular surface from the smooth facet which reflects ray r_{nj} at its i^{th} bounce. We impose the usual conditions on this function:

$$|\zeta_{ij}^{(n)}/\lambda| << 1 \tag{28a}$$

and

$$|d\zeta_{ij}^{(n)}/dx| << 1 \ . \tag{28b}$$

Equation (28a) states that the magnitude of the small-scale roughness is small compared with the acoustic wavelength. The assumption given in Eq. (28b) is that the slope of $y = \zeta_{ij}^{(n)}(x)$ is never large. Because of the restriction in Eq. (28b), the reflection coefficient on any given facet is nearly constant, with respect to grazing angle, for reflections in the specular direction.

Moreover, it has been shown that curvature of the small-scale roughness does not significantly affect the scattering of the acoustic wave,[20] so we ignore this feature here. If we assume $\zeta_{ij}^{(n)}$ to be normally distributed with mean zero over the area insonified by a ray bundle, then the coherent reflection coefficient, i.e., the reflection coefficient in the specular direction, is given by[18]

$$\tilde{B}_{ij}^{(n)} = B_{ij}^{(n)} \exp\left[-8\pi^2\sigma_{\zeta'}^2 \sin^2 \psi_{ij}^{(n)}\right] . \tag{29}$$

Here, $B_{ij}^{(n)}$ is the reflection coefficient given in Eq. (13), and $\psi_{ij}^{(n)}$ is the grazing angle, defined prior to Eq. (1), that the incident ray r_{nj} makes with the smooth facet at its i^{th} bottom reflection. The quantity $\sigma_{\zeta'}$ is the root-mean-square displacement of the surface $\zeta_{ij}^{(n)}$ from the smooth facet upon which it is superimposed, divided by the acoustic wavelength λ. We assume $\sigma_{\zeta'}$ is small by using Eq. (28a) and approximate $\tilde{B}_{ij}^{(n)}$ by

$$\tilde{B}_{ij}^{(n)} = B_{ij}^{(n)}\left(1 - 8\pi^2 \sigma_{\zeta'}^2 \sin^2 \psi_{ij}^{(n)}\right) , \tag{30}$$

to first-order terms in $\sigma_{\zeta'}^2$.

In order to incorporate Eq. (30) into our previous development, we assume that scattered waves at the receiver vanish because of their random phases. Consequently, only the wave reflected in the specular direction remains. Prior to inserting $\tilde{B}_{ij}^{(n)}$ into our equations for the mean and variance of received intensity, we regard $\sigma_{\zeta'}$ to be the same on each facet. Also, we assume they are of the same magnitude as σ_{ε}. The mean intensity then becomes

$$E(I) = \sum_{n=1}^{N} \sum_{j=1}^{4} \frac{A_{nj}^{2n}}{H^2\left(R'^2 + \bar{u}_{nj}'^2\right)} \left[1 - \frac{16\pi^2 \sigma_{\zeta'}^2 \bar{u}_{nj}'^2}{A_{nj}^2\left(R'^2 + \bar{u}_{nj}'^2\right)}\right] . \tag{31}$$

Because of our assumptions on $\sigma_{\zeta'}$, the intensity variance remains unchanged from Eq. (22), at least to second-order terms in our random variables.

In Fig. 8 we plot moment ratio M_R versus aspect ratio R' for three values of $\sigma_{\zeta'}$, 0, 0.1, and 0.2. The bottom has a mean density of 1.8 g/cm^3. The $\sigma_{\zeta'} = 0$ curve is the same as the heavy solid curve in Fig. 4, since this value of $\sigma_{\zeta'}$ corresponds to facets with no superimposed small-scale roughness. For R' = 1, varying $\sigma_{\zeta'}$ from zero to 0.2 produces about a 3 dB decrease in M_R. However, the small-scale roughness in this model is essentially inconsequential for R' greater than about four. In other words, when the grazing angle of the dominant rays becomes relatively small, the small surface variation $\zeta_{ij}^{(n)}$ has little effect, as is well known.[18] An increase in $\sigma_{\zeta'}$ causes a decrease in M_R for every value of R' in Fig. 8. This means that there is a tendency toward increased fluctuation of intensity about its mean value as $\sigma_{\zeta'}$ increases.

V. SUMMARY

This paper is concerned with the relative effects of bottom structure and topography on the intensity of a received acoustic signal. We use ray theory in a shallow-water duct having constant sound speed and density. Both the bottom sound speed and density are taken to be random in the horizontal direction. The water-bottom interface consists initially of an ensemble of large-scale two dimensional facets. Each facet is assumed to possess a small random depth deviation about a mean horizontal bottom, as well as small random slope and curvature. Acoustic rays are specularly reflected from the facet bottom.

Using perturbation expansions, we develop expressions for bottom loss and spreading loss. These results are used to derive formulas for the mean and variance of the incoherent intensity at a point receiver for a transmitted cw signal. Stochastic averaging over the bottom randomness is performed to obtain the mean and variance of intensity. The results are sufficiently general to permit their use with different bottom-acoustic models. The intensity moments are modeled to contain arbitrary correlation coefficients for each of the random variables. To

illustrate our results, we choose to use a Mackenzie bottom model and correlation coefficients of Gaussian form.

We are able to draw a number of conclusions from our results. For example, we show that the standard deviation of intensity increases as the correlation length of bottom structure or topography increases. This results from a cancelling of bottom randomness effects. Another conclusion is that varying the correlation length of the topography affects the moment ratio, the dB ratio of mean to standard deviation of intensity, more than varying that of the structure. Moreover, varying the correlation length of any of the random bottom quantities does not affect the moment ratio as much as does varying the aspect (range to depth) ratio R' does. Also, in general, for a given R' value, the moment ratio increases as the mean bottom density increases When considering with high density bottoms, the moment ratio tends to decrease as the aspect ratio increases. However, this same conclusion does not hold for low density bottoms.

We found that structural variations in the bottom make a larger contribution to intensity variance than topographical variations, when the aspect ratio is small, less than about five. For aspect ratios more than ten, topographical roughness has the greater effect. When comparing effects of the different constituents of bottom topography, it was found that curvature causes significantly greater intensity fluctuations than either depth or slope deviations. This is a consequence of the tendency of curvature to focus and defocus ray bundles. Lastly, small-scale roughness is superimposed upon the large-scale facets, and we examined the effect on intensity induced by this feature. It is found for our model that only for aspect ratios less than about five does the added roughness significantly contribute to intensity fluctuations. The small-scale roughness tends to increase variance of intnesity.

REFERENCES

1. P. J. Vidmar and R. A. Koch, "A Summary of Recent Research in Acoustic Bottom Interaction," Applied Res. Lab., The Univ. of Texas at Austin, ARL-TR-82-14 (1982).

2. F. G. Bass and I. M. Fuks, Wave Scattering from Statistically Rough Surfaces, (Pergamon Press, New York, 1979).

3. C. E. Ashley, M. J. Jacobson, and W. L. Siegmann, J. Acoust. Soc. Am. 76, 1445-1455 (1984).

4. P. A. Crowder, "Some Statistics of the Seabed and Acoustic Scattering Therefrom," in Acoustics and the Sea-Bed, edited by N. G. Pace (Bath Univ. Press, Bath, UK, 1983), pp. 147-155.

5. R. J. Urick, Principles of Underwater Sound, (McGraw-Hill, New York, 1983), pp. 272-274.

6. A. D. Seifer and M. J. Jacobson, J. Acoust. Soc. Am. 43, 1395-1403 (1968).

7. W. A. Kinney, C. S. Clay, and G. A. Sandness, J. Acoust. Soc. Am. 73, 183-194 (1983).

8. A. D. Seifer and M. J. Jacobson, J. Acoust. Soc. Am. 44, 1103-1114 (1968).

9. K. V. Mackenzie, J. Acoust. Soc. Am. 32, 221-231 (1960).

10. E. L. Hamilton, Geophysics 37, 620-646 (1972).

11. H. G. Frey, "Reflection and Scattering of Sound by the Oceah Boundaries: A Bibliography," Defense Res. Lab., The Univ. of Texas at Austin, Acoustical Report No. 285 (1967).

12. C. S. Clay and H. Medwin, "Acoustical Oceanography," (John Wiley, New York, 1977), p. 63.

13. B. F. Kur'yanov, Sov. Phys. - Acoust. 8, 252-257 (1963).

14. H. S. Hayre and D. E. Kaufman, J. Acoust. Soc. Am. 38, 599-603 (1965).

15. L. Brekhovskikh and Yu. Lysanov, Fundamentals of Ocean Acoustics (Springer-Verlag, New York, 1982), pp. 200-203.

16. S. T. MacDaniel, "Diffraction Corrections to the High-Frequency Kirchhoff Approximation," Applied Res. Lab., Penn. State Univ., State College, PA, (Jan. 1985).

17. C. E. Eckart, J. Acoust. Soc. Am. 25, 566-570 (1953).

18. C. E. Clay, J. Geophys. Res. 71, 2037-2045 (1966).

19. W. A. Kuperman, J. Acoust. Soc. Am. 58, 365-370 (1975).

20. F. H. Maltz and W. C. Meecham, J. Stat. Phys. 3, 385-394 (1971).

FIGURE LEGENDS

Fig. 1. "Actual" and "Ideal" rays for large-scale interface variations.

Fig. 2. Moment ratio M_R versus mean bottom density ρ_2 for four L' combinations: R' = 20, $\sigma_\delta = \sigma_{\mathcal{D}'} = \sigma_{\kappa'} = 1$, c_1 = 1523 m/s, ρ_1 = 1.025 g/cm^3. Surfaced source and receiver.

Fig. 3. Moment ratio M_R versus mean bottom density ρ_2 for three values of aspect ratio R': $L'_\varepsilon = L'_{\kappa'} = L'_{\mathcal{D}'} = 0$. Other parameters as in Fig. 2.

Fig. 4. Moment ratio M_R versus aspect ratio R' for three combinations of random variables: ρ_2 = 1.8 g/cm^3. Other parameters as in Fig. 3.

Fig. 5. Same as Fig. 4, except ρ_2 = 1.6 g/cm.^{3}

Fig. 6. Moment ratio M_R versus the standard deviations of bottom structure σ_ε and curvature $\sigma_{\kappa'}$: R' = 10, ρ_2 = 1.8 g/cm^3. Other parameters as in Fig. 3.

Fig. 7. Moment ratio M_R versus mean bottom density ρ_2 and aspect ratio R'. Other parameters as in Fig. 3.

Fig. 8. Moment ratio M_R versus aspect ratio R' for three values of σ'_ζ: ρ_2 = 1.8 g/cm^3. Other parameters as in Fig. 3.

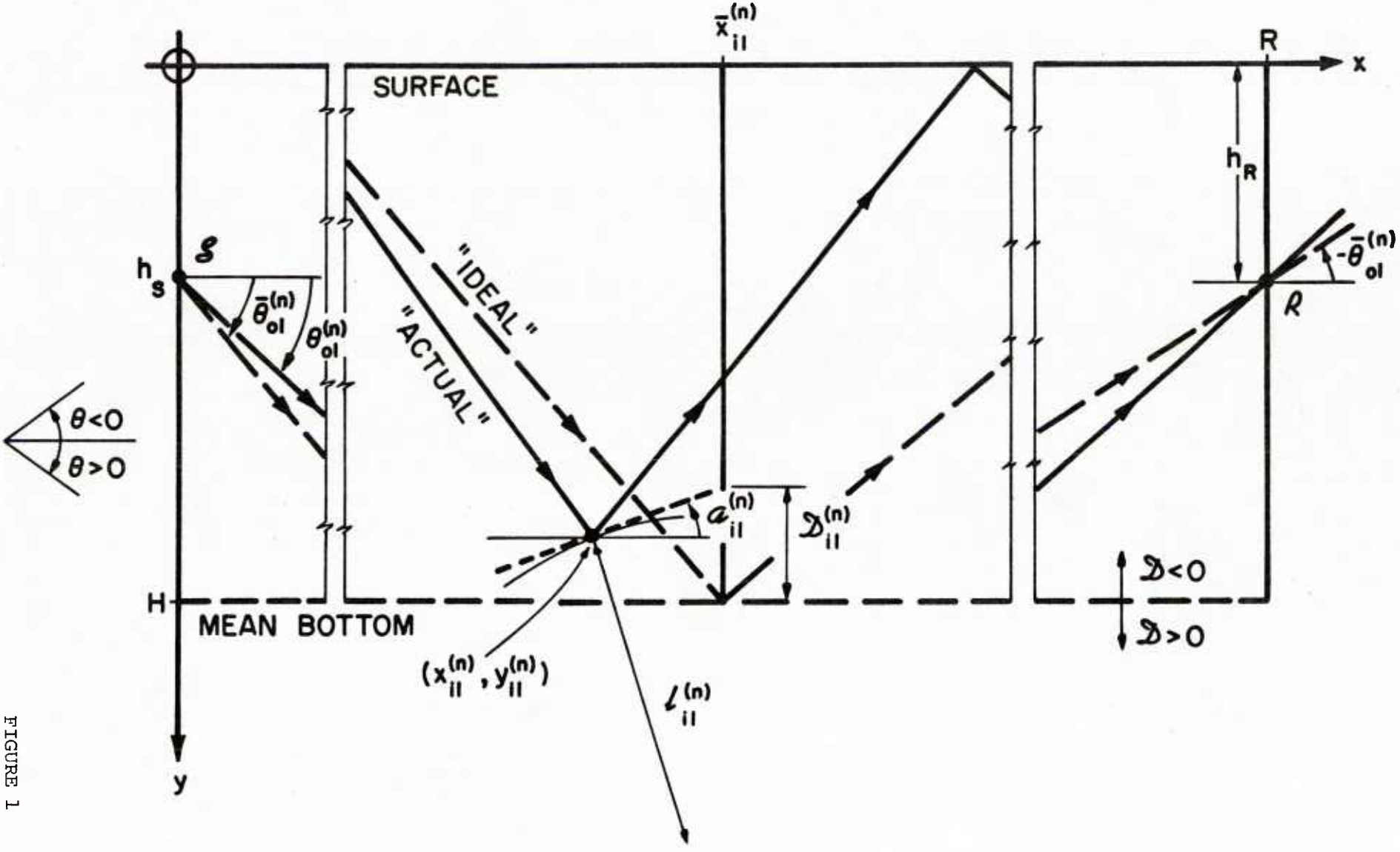
SURFACE
MEAN BOTTOM
"IDEAL"
"ACTUAL"
R
x
y
H
h_s
h_R
$\bar{x}_{il}^{(n)}$
$\bar{\theta}_{ol}^{(n)}$
$\theta_{ol}^{(n)}$
$-\bar{\theta}_{ol}^{(n)}$
$\alpha_{il}^{(n)}$
$\mathcal{D}_{il}^{(n)}$
$(x_{il}^{(n)}, y_{il}^{(n)})$
$\ell_{il}^{(n)}$
$\theta<0$
$\theta>0$
$\mathcal{D}<0$
$\mathcal{D}>0$

FIGURE 1

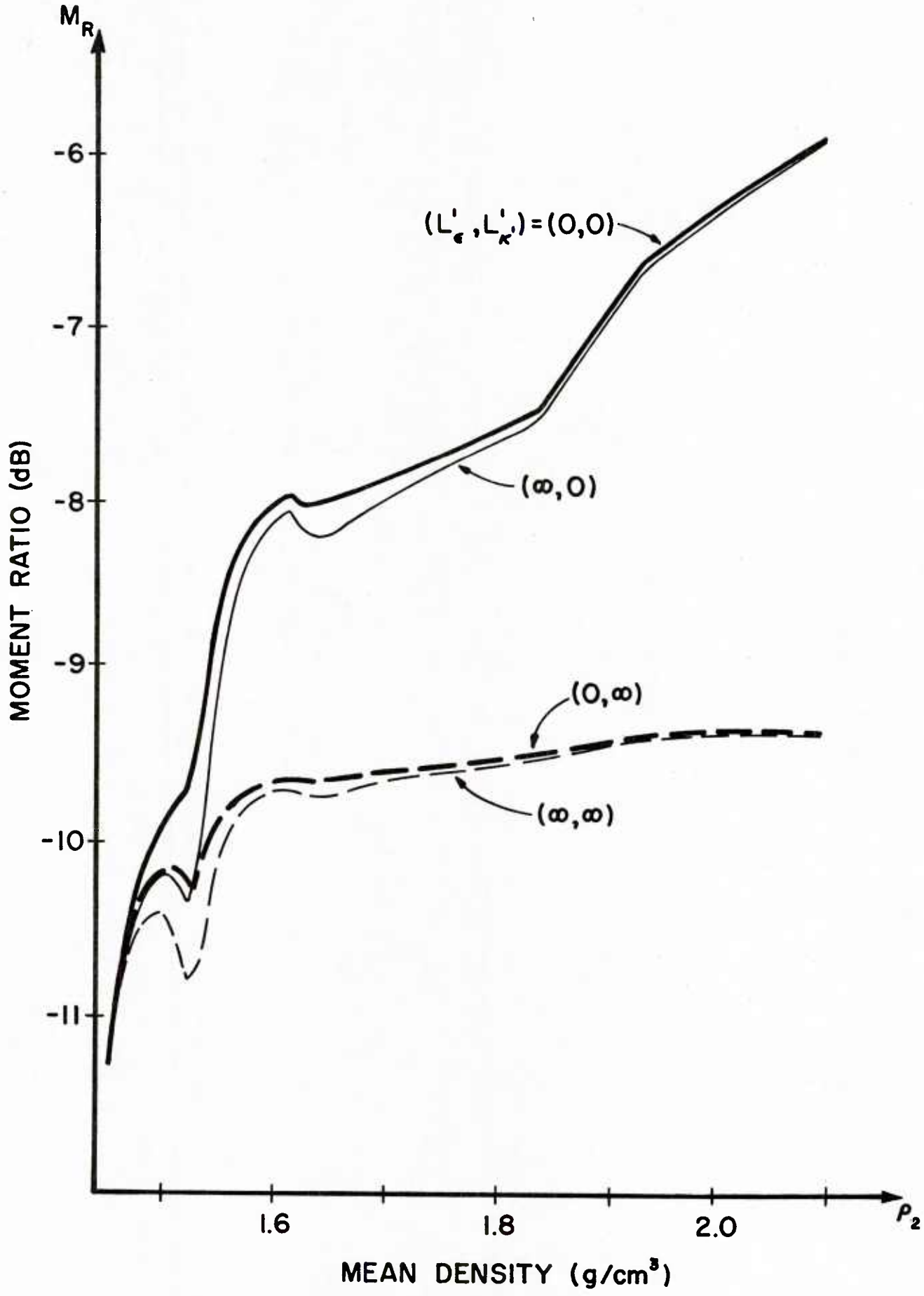
M_R
-6
-7
-8
-9
-10
-11
MOMENT RATIO (dB)
$(L'_\epsilon, L'_\kappa) = (0,0)$
$(\infty, 0)$
$(0, \infty)$
(∞, ∞)
1.6
1.8
2.0
ρ_2
MEAN DENSITY (g/cm³)

FIGURE 2

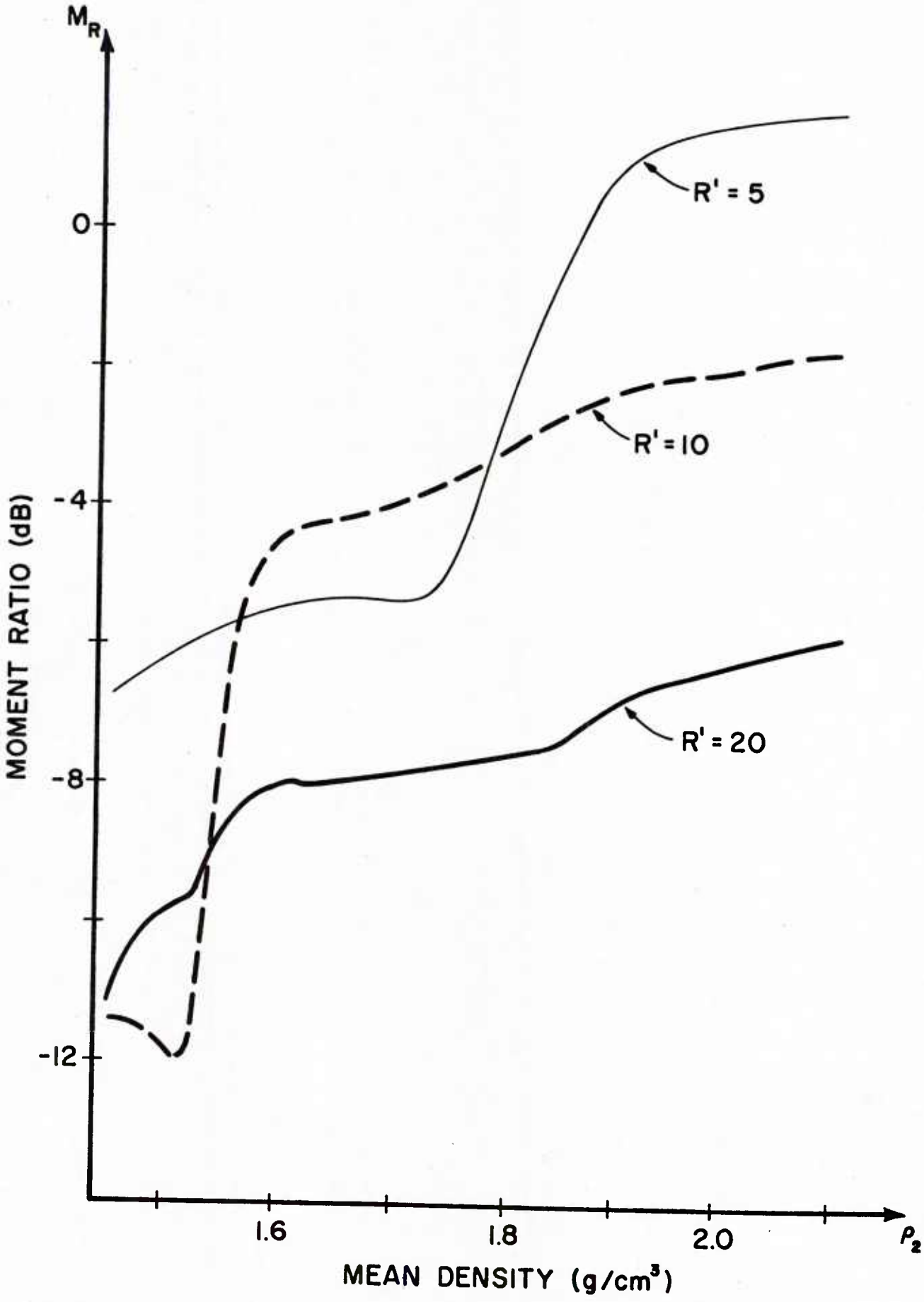
M_R
0
-4
-8
-12
MOMENT RATIO (dB)
R' = 5
R' = 10
R' = 20
1.6
1.8
2.0
ρ_2
MEAN DENSITY (g/cm³)

FIGURE 3

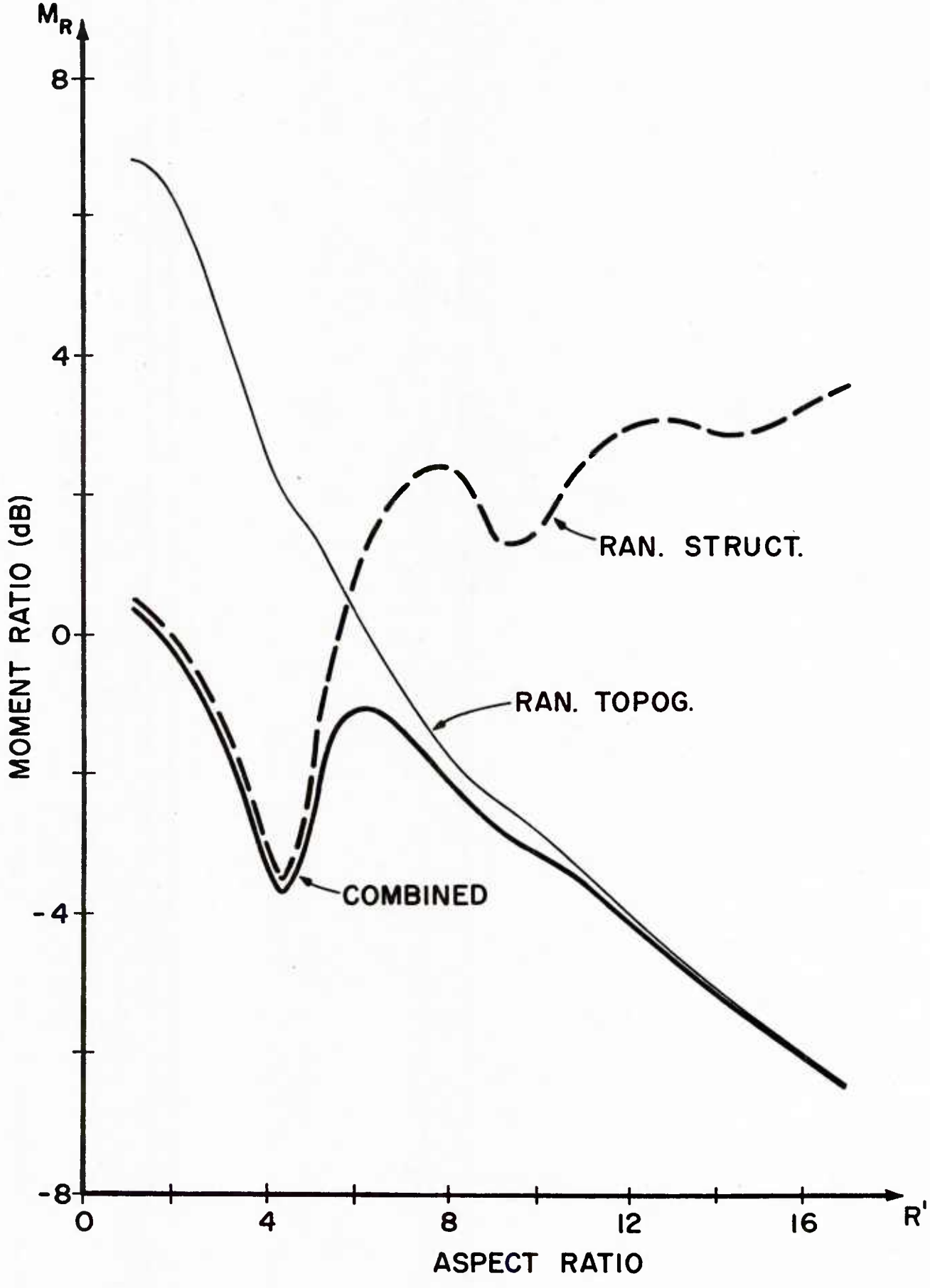
M_R
8
4
0
-4
-8
MOMENT RATIO (dB)
RAN. STRUCT.
RAN. TOPOG.
COMBINED
0
4
8
12
16
R'
ASPECT RATIO

FIGURE 4

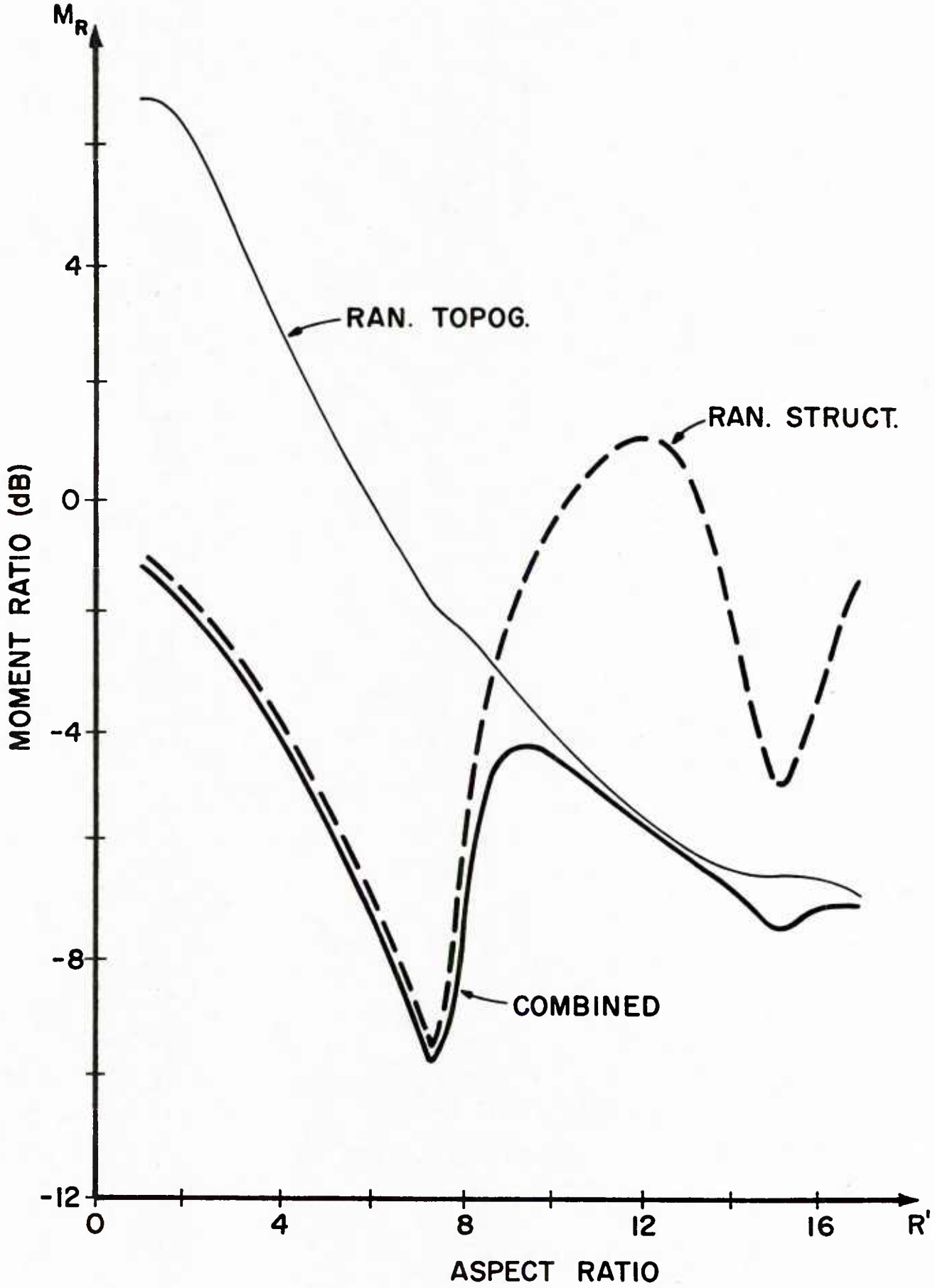
M_R
4
0
-4
-8
-12
MOMENT RATIO (dB)
RAN. TOPOG.
RAN. STRUCT.
COMBINED
0
4
8
12
16
R'
ASPECT RATIO

FIGURE 5

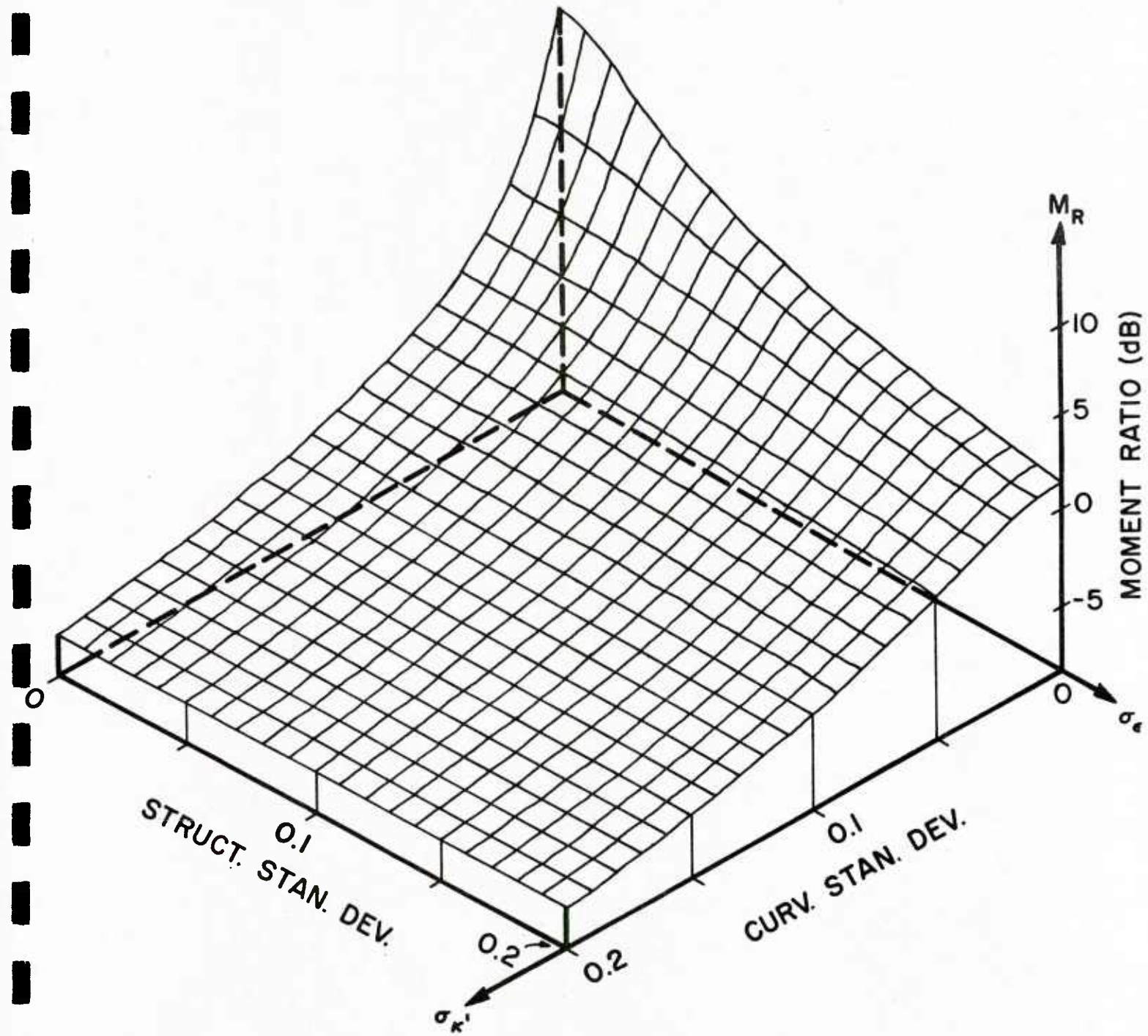
M_R
10
5
0
-5
MOMENT RATIO (dB)
0
0.1
STRUCT. STAN. DEV.
0.2
$\sigma_{\kappa'}$
0
0.1
CURV. STAN. DEV.
0.2
σ_ϕ

FIGURE 6

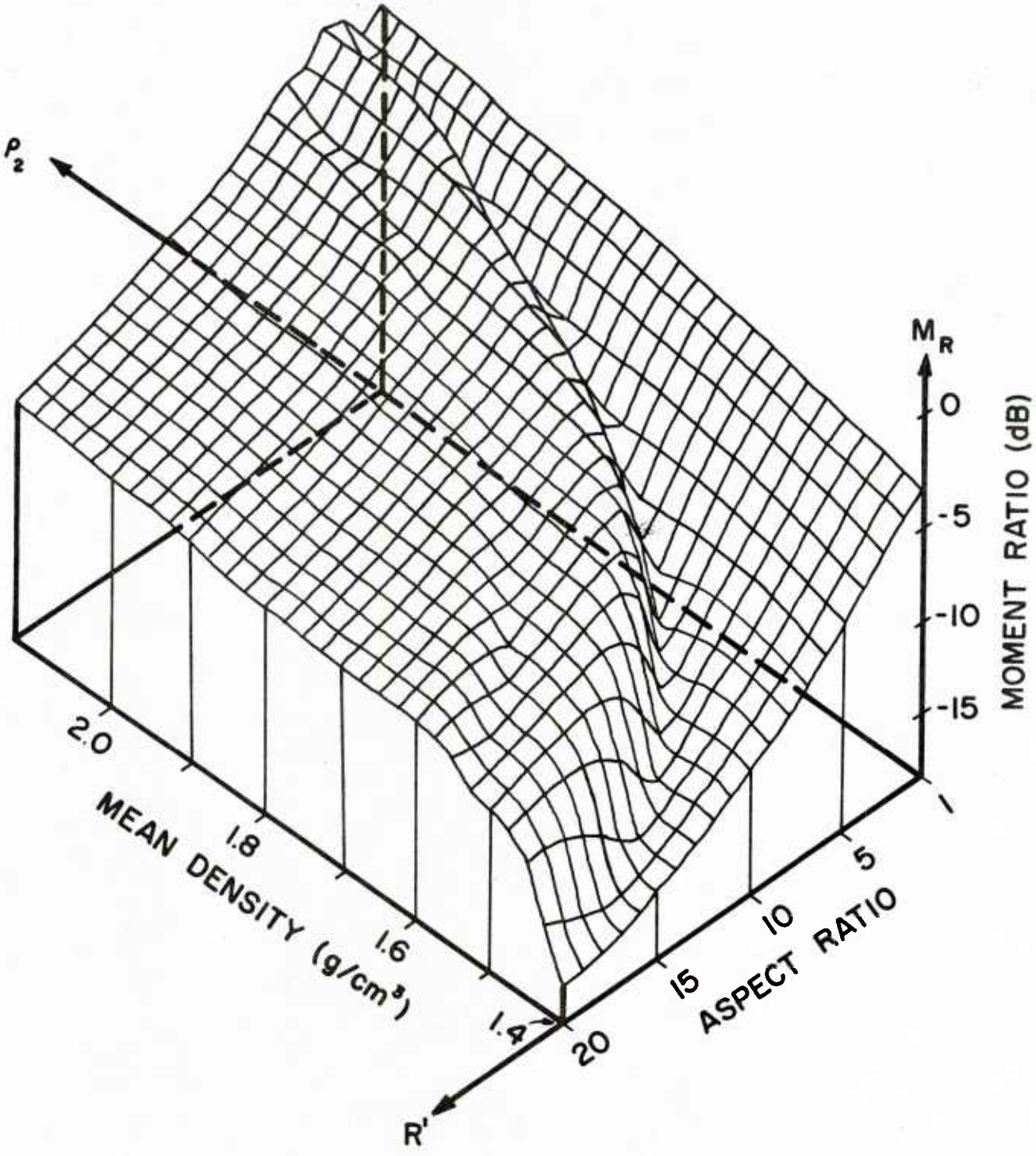
ρ_2
M_R
0
-5
-10
-15
MOMENT RATIO (dB)
2.0
1.8
1.6
1.4
MEAN DENSITY (g/cm³)
1
5
10
15
20
ASPECT RATIO
R'

FIGURE 7

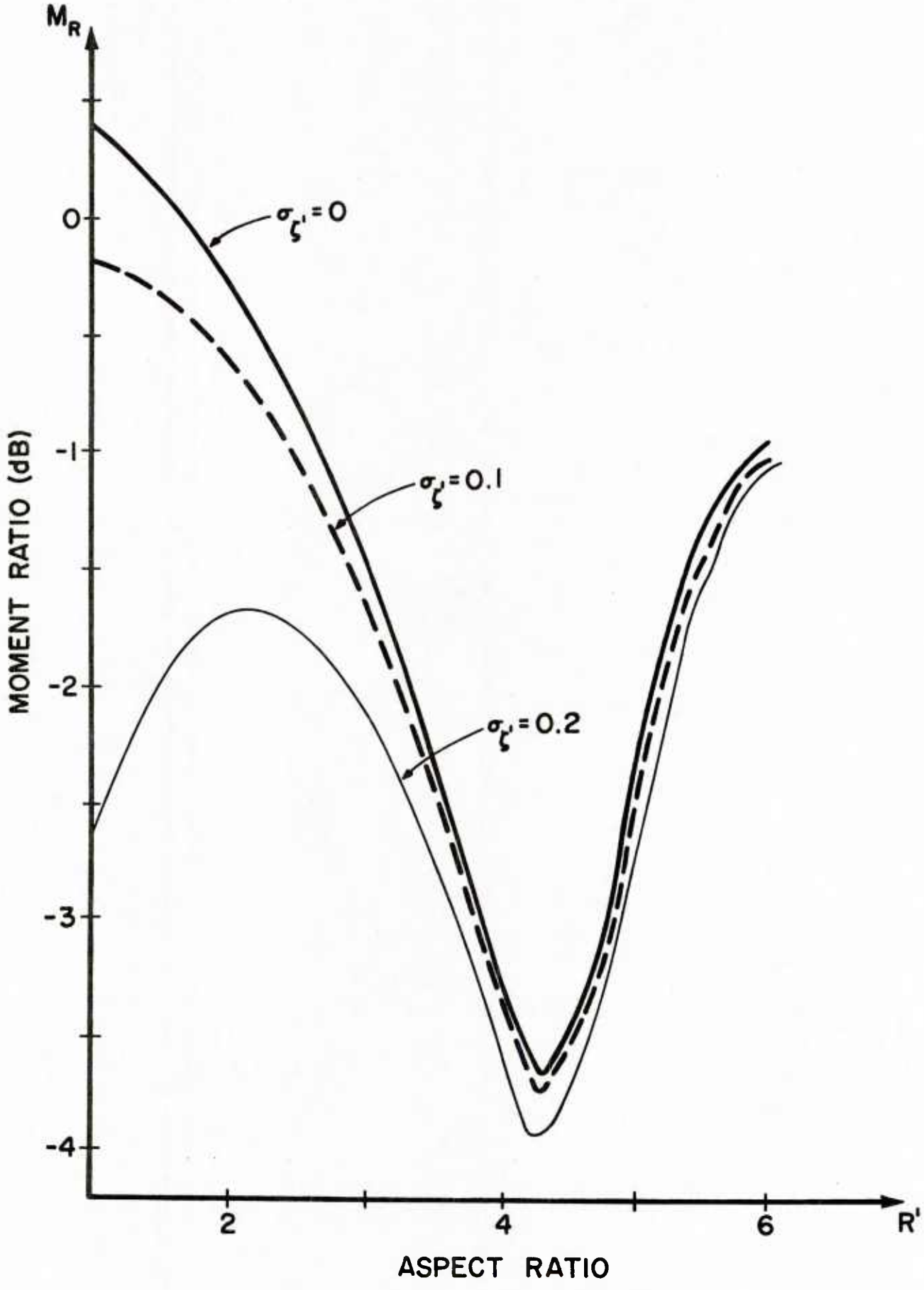
M_R
0
-1
-2
-3
-4
MOMENT RATIO (dB)
$\sigma_{\zeta'} = 0$
$\sigma_{\zeta'} = 0.1$
$\sigma_{\zeta'} = 0.2$
2
4
6
R'
ASPECT RATIO

FIGURE 8

UNCLASSIFIED
DISTRIBUTION LIST
DEC 1981

Addressee	No. of Copies
Office of Naval Research 800 North Quincy Street Arlington, Virginia 22217	
Attn: Code 425AC	2
102	1
102C	1
210	1
220	1
Office of Naval Technology 800 North Quincy Street Arlington, Virginia 22217	
Attn: MAT 0721	1
MAT 0724	1
Director Naval Research Laboratory 4555 Overlook Avenue, SW. Washington, D.C. 20375	
Attn: Dr. J. C. Munson	1
Mr. R. R. Rojas	1
Dr. B. B. Adams	1
Dr. W. B. Moseley	1
Dr. J. P. Dugan	1
Unclassified Library	1
Superintendent Naval Research Laboratory Underwater Sound Reference Division P.O. Box 8337 Orlando, Florida 32806	1
Director Office of Naval Research Branch Office 1030 East Green Street Pasadena, California 91106	1
Office of Naval Research Rm 239, Campbell Hall University of California Berkeley, California 94720	1
Director Office of Naval Research Branch Office 495 Summer Street Boston, Massachusetts 02210	1
Office of Naval Research New York Area Office 715 Broadway - 5th Floor New York, New York 10003	1
Commanding Officer Office of Naval Research Branch Office Box 39 FPO New York 09510	1
Director Office of Naval Research Branch Office 536 South Clark Street Chicago, Illinois 60605	1
Office of Naval Research Resident Representative University District Building, Room 422 1107 North East 45th Street Seattle, Washington 98105	1

Addressee	No. of Copies
Technical Director Naval Oceanographic Research and Development Activity NSTL Station Bay St. Louis, Mississippi 39522	
Attn: Technical Director	1
Dr. L. Solomon	1
Dr. R. Gardner	1
Mr. E. Chaika	1
Mr. R. Van Wyckhouse	1
Dr. S. W. Marshall	1
Director Naval Oceanographic Office NSTL Station Bay St. Louis, Mississippi 39522	
Attn: Mr. H. Beck	1
Dr. T. M. Davis	1
Mr. W. H. Geddes	1
Dr. W. Jobst	1
Mr. R. Merrifield	1
Mr. R. A. Peloquin	1
Dr. M. K. Shank	1
Office of the Assistant Secretary of the Navy for Research, Engineering and Systems Washington, D.C. 20350	
Attn: Dr. D. Barbe, Rm 4E732 Pentagon	1
Dr. J. H. Probus, Rm 5E779 Pentagon	1
Chief of Naval Operations Room 5D580, Pentagon Washington, D.C. 20350	
Attn: OP951F	1
Commander Naval Sea Systems Command Department of Navy Washington, D.C. 20362	
Attn: Capt. James M. Van Metre PMS 409	1
Chief of Naval Operations Office of the Director Naval Oceanographic Division OP-952 Department of the Navy Washington, D.C. 20352	
Attn: Dr. R. W. James	1
Capt. J. C. Harlett	1
Commander Oceanographic System, Atlantic Box 100 Norfolk, Virginia 23511	1
Commander Oceanographic System, Pacific Box 1390 Pearl Harbor, Hawaii 96860	1

Addressee	No. of Copies
Defense Advanced Research Projects Agency 1400 Wilson Boulevard Arlington, Virginia 22209 Attn: Capt. V. Simmons	1
ARPA Research Center Moffett Field Unit #1 California 94035 Attn: Mr. E. Smith	1
Commanding Officer Fleet Weather Central Box 113 Pearl Harbor, Hawaii 96860	1
Naval Ocean Systems Center (Kaneohe) Kaneohe, Hawaii 96863 Attn: Mr. D. Hightower Mr. B. Kishimoto Mr. R. Buecher	1 1 1
Commander Naval Electronic Systems Command 2511 Jefferson Davis Highway National Center #1 Arlington, Virginia 20360 Attn: CAPT C. A. Rose,, PME 124 LCDR P. Girard, NAVELEX 612	2
Commander Naval Air Systems Command Jefferson Plaza #1 1411 Jefferson Davis Highway Arlington, Virginia 20360	1
Commander Naval Sea Systems Command National Center #2 2521 Jefferson Davis Highway Arlington, Virginia 20362 Attn: SEA 63R 63Y	1 1
Commanding Officer Fleet Numerical Weather Central Monterey, California 93940 Attn: Mr. Paul Stevens Dr. D.R. McLain (NMFS)	1 1
Defense Documentation Center Cameron Station Alexandria, Virginia 22314	12
Commander Naval Ocean Systems Center Department of the Navy San Diego, California 92132 Attn: Dr. Daniel Andrews Dr. Dean Hanna Mr. Henry Aurand Dr. Harry A. Schenck	1 1 1 1

Addressee	No. of Copies
Commander Naval Surface Weapons Center Acoustics Division Silver Spring, Maryland 20910	1
Commander Naval Surface Weapons Center Science and Mathematics Research Group (K05) Dahlgren, Virginia 22448 Attn: Dr. E.W. Schwiderski	1
Commanding Officer Naval Underwater Systems Center New London Laboratory New London, Connecticut 06320 Attn: Dr. William Von Winkle Dr. A. Nuttall Mr. A. Ellinthorpe Dr. D.M. Viccione Mr. A. Donn Cobb	1 1 1 1 1
Commander Naval Air Development Center Department of the Navy Warminster, Pennsylvania 18974 Attn: Unclassified Library	1
Commanding Officer Naval Coastal Systems Laboratory Panama City, Florida 32401 Attn: Unclassified Library	1
Commanding Officer Naval Underwater Systems Center Newport Laboratory Newport, Rhode Island 02840 Attn: Unclassified Library	1
Commander David W. Taylor Naval Ship Research and Development Center Bethesda, Maryland 20084 Attn: Dr. M. Sevik	1
Superintendent Naval Postgraduate School Monterey, California 93940	1
Superintendent U.S. Naval Academy Annapolis, Maryland 21402 Attn: Library	1
Commanding Officer Naval Intelligence Support Center 4301 Suitland Road Washington, D.C. 20390 Attn: NISC 20	1
Director Applied Physics Laboratory University of Washington 1013 North East 40th Street Seattle, Washington 98105 Attn: Dr. T.E. Ewart Dr. M. Schulkin	1 1

Addressee	No. of Copies
Applied Research Laboratories University of Texas at Austin P.O. Box 8029 10000 FM Road 1325 Austin, Texas 78712	
Attn: Dr. Loyd Hampton	1
Dr. Charles Wood	1
Atlantic Oceanographic and Meteorological Laboratories 15 Rickenbacker Causeway Miami, Florida 33149	
Attn: Dr. John Proni	1
Bell Telephone Laboratories 1 Whippany Road Whippany, New Jersey 07981	
Attn: Dr. Bruce Bogart	1
Dr. Peter Hirsch	1
Bolt, Beranek, and Newman, Inc. 50 Moulton Street Cambridge, Massachusetts 02238	
Attn: Dr. K. L. Chandiramani	1
Chase, Inc. 14 Pinckney Street Boston, Massachusetts 02114	
Attn: Dr. David Chase	1
Dr. David Middleton 127 East 91st Street New York, New York 10028	1
Duke University Department of Electrical Engineering Durham, North Carolina 27706	
Attn: Dr. Loren Nolte	1
General Electric Company Heavy Military Electronic Systems Syracuse, New York 13201	
Attn: Mr. Don Winfield	1
General Electric Company P.O. Box 1088 Schenectady, New York 12301	
Attn: Dr. Thomas G. Kincaid	1
Gould, Incorporated Chesapeake Instrument Division 5711 Baymeadow Drive Glen Burnie, Maryland 21061	
Attn: Dr. O. Lindemann	1
G R Associates, Inc. 10750 Columbia Pike Suite 602 Silver Spring, Maryland 20901	
Attn: Dr. Sheldon Gardner	
Dr. Frank Rees	
Hughes Aircraft Company P.O. Box 3310 Fullerton, California 92634	
Attn: Mr. S. W. Autrey	1

Addressee	No. of Copies
Hydroacoustics, Inc. 321 Northland Ave. P.O. Box 3818 Rochester, New York 14610	1
Institute for Acoustical Research Miami Division for the Palisades Geophysical Institute 615 South West 2nd Avenue Miami, Florida 33130	
Attn: Mr. M. Kronengold	1
Dr. J. Clark	1
Institute of Geophysics and Planetary Physics Scripps Institute of Oceanography University of California La Jolla, California 92093	
Attn: Dr. W. Munk	1
Mr. J. Spiesberger	1
Jaycor Incorporated 205 South Whiting Street Suite 607 Alexandria, Virginia 22304	
Attn: Dr. S. Adams	1
Massachusetts Institute of Technology Acoustics and Vibration Laboratory 70 Massachusetts Avenue Room 5-222 Cambridge, Massachusetts 02139	
Attn: Professor Patrick Leehey	1
Palisades Sofar Station Bermuda Division of Palisades Geophysical Institute FPO New York 09560	
Attn: Mr. Carl Hartdegen	1
Polar Research Laboratory 123 Santa Barbara Avenue Santa Barbara, California 93101	
Attn: Mr. Beaumont Buck	1
Research Triangle Institute Research Triangle Park Durham, North Carolina 27709	
Attn: Dr. S. Huffman	1
Rensselaer Polytechnic Institute Troy, New York 12181	
Attn: Dr. Melvin J. Jacobson	
Science Applications, Inc. 8400 Westpark Drive McLean, Virginia 22102	
Attn: Dr. P. Tatro	
S.D.P. Inc. 15250 Ventura Boulevard Suite 518 Sherman Oaks, California 91403	
Attn: Dr. M. A. Basin	1

Addressee	No. of Copies
Texas Instruments, Inc. 13500 North Central Expressway Dallas, Texas 75231 Attn: Mr. Charles Black	1
Underwater Systems, Inc. 8121 Georgia Avenue Silver Spring, Maryland 20910 Attn: Dr. M. Weinstein	1
University of Miami Rosenstiel School of Marine and Atmospheric Sciences 4600 Rickenbacker Causeway Miami, Florida 33149 Attn: Dr. H. DeFerrari	1
University of Michigan Department of Aerospace Engineering, North Campus Ann Arbor, Michigan 48109 Attn: Dr. W. W. Wilmarth	
University of Michigan Cooley Electronics Laboratory Ann Arbor, Michigan 48105 Attn: Dr. T. G. Birdsall	
University of Rhode Island Department of Electrical Engineering Wakefield, Rhode Island 02881 Attn: Dr. Donald Tufts	1
Woods Hole Oceanographic Institution Woods Hole, Massachusetts 02543 Attn: Dr. Paul McElroy Dr. R. Spindel	1 1